Ocean Convective Available Potential Energy. Part I: Concept and Calculation

ZHAN SU AND ANDREW P. INGERSOLL

Division of Geological and Planetary Sciences, California Institute of Technology, Pasadena, California

ANDREW L. STEWART

Department of Atmospheric and Oceanic Sciences, University of California, Los Angeles, Los Angeles, California

ANDREW F. THOMPSON

Environmental Science and Engineering, California Institute of Technology, Pasadena, California

(Manuscript received 1 August 2014, in final form 11 January 2016)

ABSTRACT

Thermobaric convection (type II convection) and thermobaric cabbeling (type III convection) might substantially contribute to vertical mixing, vertical heat transport, and deep-water formation in the World Ocean. However, the extent of this contribution remains poorly constrained. The concept of ocean convective available potential energy (OCAPE), the thermobaric energy source for type II and type III convection, is introduced to improve the diagnosis and prediction of these convection events. OCAPE is analogous to atmospheric CAPE, which is a key energy source for atmospheric moist convection and has long been used to forecast moist convection. OCAPE is the potential energy (PE) stored in an ocean column arising from thermobaricity, defined as the difference between the PE of the ocean column and its minimum possible PE under adiabatic vertical parcel rearrangements. An ocean column may be stably stratified and still have nonzero OCAPE. The authors present an efficient strategy for computing OCAPE accurately for any given column of seawater. They further derive analytical expressions for OCAPE for approximately two-layer ocean columns that are widely observed in polar oceans. This elucidates the dependence of OCAPE on key physical parameters. Hydrographic profiles from the winter Weddell Sea are shown to contain OCAPE ($0.001–0.01\ J\ kg^{-1}$), and scaling analysis suggests that OCAPE may be substantially enhanced by wintertime surface buoyancy loss. The release of this OCAPE may substantially contribute to the kinetic energy of deep convection in polar oceans.

1. Introduction

Deep-water formation in the Labrador, Greenland, and Mediterranean Seas is the result of open-ocean deep convection (Schott and Leaman 1991; Clarke and Gascard 1983; Marshall and Schott 1999; Harcourt et al. 2002). Formation of Antarctic Bottom Water (AABW) is induced either by deep convection or by processes occurring around the continental margins (Gordon 1978). Deep convection significantly contributes to the global ocean overturning circulation and has a prominent influence on the global transport of heat, salt, and nutrients (Macdonald and Wunsch 1996).

Akitomo (1999a,b) classified ocean deep convection into two types. The first type (type I) is the convection of a ''gradually deepening mixed layer'' in a nearly homogeneous ocean, driven mainly by a continuous negative surface buoyancy flux and other preconditioning processes. The second type (type II) is thermobaric convection. The term thermobaricity refers to the thermal expansion coefficient of seawater increasing with pressure, which is larger near the freezing point than at higher temperatures (McDougall 1987). Harcourt (2005) was the first to simulate type III convection, also called thermobaric cabbeling, which involves strong modulation from cabbeling as well as thermobaricity. Type II convection involves plumes of cold freshwater (CFW) sinking into warm salty water (WSW). Type III

Corresponding author address: Zhan Su, Division of Geological and Planetary Sciences, California Institute of Technology, 1200 E. California Blvd., Pasadena, CA 91125.
E-mail: zssu@caltech.edu

DOI: 10.1175/JPO-D-14-0155.1

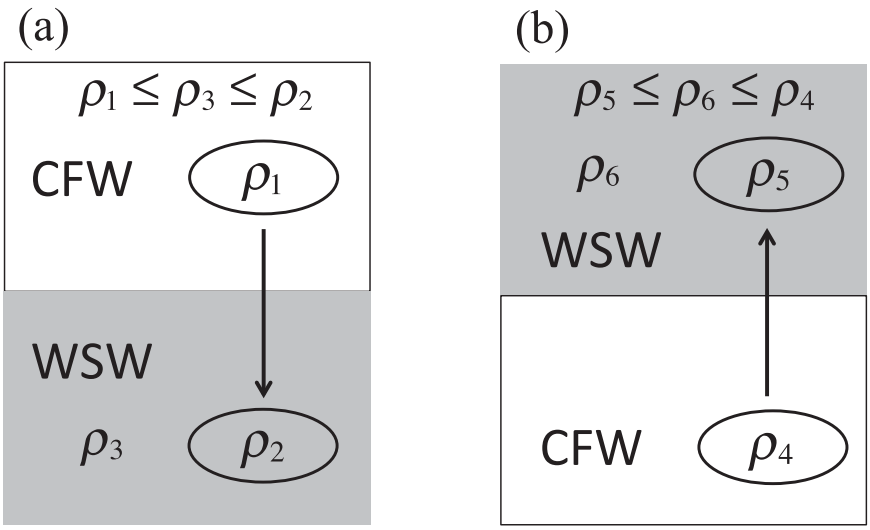

FIG. 1. Illustration of thermobaric instability by an adiabatic parcel displacement from the CFW to the WSW (a) when CFW lies above WSW or (b) when CFW lies below WSW, detailed in section 1.

convection involves convective plumes of a CFW–WSW mixture sinking into WSW due to cabbeling instability (Harcourt 2005). Cabbeling instability is a convective phenomenon that occurs when water masses with different temperatures are mixed diabatically to produce a water mass with greater density than the parent waters (Carmack 1979). For both types, thermobaricity and cabbeling are critical for the acceleration of convective plumes by generating negative buoyancy anomalies. Note that "cabbeling" in this manuscript always means the quadratic dependency of water density on potential temperature (McDougall 1987).

Harcourt (2005) suggested that type III convection may be responsible for thick, deep internal layers and localized "chimney" structures observed in the Weddell Sea. Akitomo (2006) suggested that the overturning of type II convection may penetrate to a depth of about 1.5 km on the flanks of the Maud Rise in the Weddell Sea. Type II and type III convection may contribute to the observed water properties and velocities ($\sim$10 cm s^{-1}) of convective plumes in the Greenland Sea (Akitomo 2011; Denbo and Skyllingstad 1996). Type II and type III convection may also be formation mechanisms for certain open-ocean Weddell Polynyas due to their ability to transport heat rapidly upward resulting in sea ice melt (McPhee 2000, 2003; Harcourt 2005; Akitomo 2007).

In this paper, we focus on the effect of thermobaricity only. As illustrated in Fig. 1a (Fig. 1b), for a column that is stably stratified, the movement of a parcel of CFW, or a CFW–WSW mixture, downward (upward) through the WSW adiabatically may lead to the density of that parcel becoming greater (smaller) than that of the surrounding WSW. This is a result of the thermobaric effect; the effect of temperature on density increases with depth, so the CFW may become denser (less dense) than the WSW at depth (height). In this case, potential energy (PE) will be released as the parcel sinks (rises) further. Note that moving a WSW parcel up (down) through the CFW never leads to a lower PE state. This is because the WSW parcel loses (gains) buoyancy relative to the CFW as it rises (sinks). Therefore, both type II and type III convection have an important source of kinetic energy (KE) that comes from the stored PE of the ocean column due to thermobaricity.

In this paper and its companion (Su et al. 2016, hereinafter Part II), we define and investigate a new concept, the ocean convective available potential energy (OCAPE) as an energy source for type II and type III convection due to thermobaricity. In this first paper, we focus on the conceptual importance of OCAPE and provide examples of its amplitude based on observations in the Weddell Sea. Dynamical analyses relevant to the OCAPE release and its transformation efficiency into KE are presented in Part II. In Part II, we also evaluate the KE contribution to type II and type III convection due to diabatic processes (e.g., effects due to cabbeling and stratification).

OCAPE is conceptually important: it parallels atmospheric convective available potential energy (CAPE), a key energy source in atmospheric moist convection that has long been used to forecast moist convection (see, e.g., chapter 7.4.1 of Salby 1996; Arakawa and Schubert 1974; Emanuel et al. 1994; Trenberth 2005; Zhang 2009). Both CAPE and OCAPE measure the maximum stored

PE that can be released under adiabatic vertical parcel rearrangements.[1] CAPE arises from moisture in the lower atmosphere, whereas OCAPE arises from the ocean stratification with CFW lying above or below WSW. CAPE is released when moist air parcels gain buoyancy via the release of latent heat, when they are perturbed upward and saturate at a critical pressure. OCAPE is released when parcels of CFW, or a CFW–WSW mixture, lose (gain) buoyancy via thermobaricity, when they are moved down (up) through the WSW layer past a critical depth. CAPE can be calculated by comparing the adiabatic lapse rate of moist parcels with the background temperature profile (Salby 1996). OCAPE can be calculated by the strategy developed in this paper. CAPE is widely used in subgrid-scale convective parameterization closures in atmospheric general circulation models (GCMs) (Zhang and McFarlane 1995; Gregory et al. 2000). OCAPE might be similarly useful to improve the subgrid-scale parameterizations of type II and type III convection in present ocean GCMs, as demonstrated in this paper and Part II.

In section 2, we quantitatively define OCAPE, which is the maximal PE, including internal energy and gravitational energy, of an ocean column available to be transformed into KE by vertical adiabatic parcel rearrangements. OCAPE is similar to available potential energy (APE) in the sense that they are both based on adiabatic parcel rearrangements and are both based on the global minimum PE state. However, OCAPE arises from thermobaricity, whereas APE arises mainly from baroclinicity (for APE, see Winters et al. 1995; Huang 2005; Vallis 2006). In section 3, we develop an accurate strategy to compute OCAPE, which is applicable to any vertical profile of seawater. In section 4, we derive analytical expressions for OCAPE in approximately two-layer profiles to elucidate the dependence of OCAPE on key parameters in the real ocean. In section 5, we investigate OCAPE in the Weddell Sea using hydrographic profiles. Section 6 comprises our discussion and conclusions.

2. Definition of ocean convective available potential energy

A system tends to deform to minimize its PE according to the principle of minimum total potential energy (e.g., Reddy 2002). For most complex systems, there is one state of global minimum PE and many states of local minimum PE in which the system can reside. This is true for ocean columns because of the nonlinear equation of state (EOS) of seawater (see section 3 for details). Specifically, stably stratified profiles of temperature and salinity may not be equivalent to a global minimum PE state. For these profiles, type II or type III convection may release PE and evolve the system from a state of local minimum PE into a state of lower local minimum PE or even global minimum PE. Note that the states of local or global minimum PE may be modified significantly by diabatic processes that typically occur during the convection.

In this paper, we follow the definition of APE, a key concept for ocean mesoscale geostrophic turbulence, to define OCAPE. APE is defined as the maximal PE that can be released by adiabatic parcel rearrangements, arising mainly from the baroclinicity of the system.[2] OCAPE is defined for an ocean column (i.e., without horizontal inhomogeneity and thus without baroclinicity) as the maximal PE that can be released by adiabatic vertical parcel rearrangements, arising from thermobaricity. We use the term ''reference state'' with regard to the state of global minimum PE that can be reached by adiabatic parcel rearrangements from the ''current state.'' Therefore, our definition of OCAPE is

$$\mathrm{OCAPE} = \mathrm{PE\,(current\ state)} - \mathrm{PE\,(reference\ state)}, \tag{1}$$

where PE includes gravitational energy and internal energy. As mentioned above, the reference state (and thus OCAPE) may evolve over time if water properties are modified diabatically during convection. In other words, all the terms in (1) may be a function of time. We investigate this effect of diabatic processes for OCAPE (and type II and type III convection) in Part II.

Calculating OCAPE directly using (1) is awkward because PE is not a thermodynamic variable. For a single column with the bottom at a constant level z_{bot}, PE can be generally defined as

$$\frac{\mathrm{PE}}{\mathrm{area}} = \int_{z_{\mathrm{bot}}}^{z_{\mathrm{top}}} (U + gz)\rho\, dz + z_{\mathrm{top}} P_{\mathrm{top}}, \tag{2}$$

where U is the internal energy, gz is the gravitational energy with g constant, $z_{\mathrm{top}}P_{\mathrm{top}}$ is the work done by atmospheric pressure on the column, and z_{top} is the level

[1] An adiabatic process in this paper always refers to a reversible process with no viscous dissipation and no exchanges of heat and salt.

[2] See section 3.10 of Vallis (2006), section 2b of Huang (2005), and section 3 of Winters et al. (1995).

of the ocean surface. By inserting the hydrostatic balance $\int_{z_{bot}}^{z_{top}} gz\rho\, dz = -zP|_{bot}^{top} + \int_{z_{bot}}^{z_{top}} P\, dz$ into (2), we obtain

$$\frac{\text{PE}}{\text{area}} = \int_{z_{bot}}^{z_{top}} (U + P/\rho)\rho\, dz + z_{bot}P_{bot} = H + z_{bot}P_{bot}, \tag{3}$$

where $(U + P/\rho)$ is the specific enthalpy and $H = \int_{z_{bot}}^{z_{top}} (U + P/\rho)\rho\, dz$ is the total enthalpy of the column per unit area. For an isolated column with a fixed bottom, $z_{bot}P_{bot}$ is constant during convection because of mass conservation. Thus, from (3) we can use column enthalpy to represent column PE, consistent with Reid et al. (1981). Therefore, OCAPE can also be defined as

$$\text{OCAPE} = H\,(\text{current state}) - H\,(\text{reference state}). \tag{4}$$

Here, OCAPE has dimensions of energy/area; later for convenience we also use dimensions of energy/mass for OCAPE (column averaged). Enthalpy is a thermodynamic variable and is therefore easier to diagnose than PE for both theoretical and numerical studies. Given the vertical profiles of temperature and salinity of an ocean column, we can calculate the column enthalpy directly, for example, using the Gibbs function (Feistel 2003).

For a stably or neutrally stratified ocean column ($N^2 \geq 0$), the existence of OCAPE is entirely due to thermobaricity. To demonstrate this, we perform the following thought experiment: First, note that the salinity contraction coefficient is nearly independent of pressure (as shown in section 4a), that is, the density satisfies $\partial^2\rho/\partial S\partial P|_\theta \approx 0$, where S and θ are salinity and potential temperature, respectively. If there is no thermobaricity, that is, $\partial^2\rho/\partial\theta\partial P|_S = 0$, then the adiabatic compressibility $\partial\rho/\partial P$ is independent of θ and S. Therefore, ρ must have the form $\rho = \rho_1(\theta, S) + \rho_2(P)$, and ρ_1 increases monotonically with depth since $N^2 \geq 0$ here.[3] Therefore, any exchange of parcels with different ρ_1 leads to an unstable stratification, as the rearrangement necessarily leads to a nonmonotonic profile of ρ_1 with depth. Now we demonstrate that in this scenario the PE (or enthalpy) of the system cannot be reduced by adiabatically swapping the positions of any parcels of equal mass. First, note that in general any parcel rearrangement can be decomposed into a series of equal-mass two-parcel exchanges. For adiabatic exchanges there is no change in entropy or salinity, so the variation of specific enthalpy $d\eta$ of any exchanged parcel is dP/ρ. We denote the swapped parcels as i and j with equal masses m, and their initial pressures as P_i and P_j, where $P_i < P_j$. It may be shown that the change in the system's enthalpy associated with the exchange is

$$m\int_{P_j}^{P_i}\left[\frac{1}{\rho_1(\theta_j, S_j) + \rho_2(P)} - \frac{1}{\rho_1(\theta_i, S_i) + \rho_2(P)}\right] dP. \tag{5}$$

This quantity is always positive or zero because $\rho_1(\theta_j, S_j) \geq \rho_1(\theta_i, S_i)$ and $dP < 0$. Thus, any parcel exchanges cannot decrease the system's enthalpy, and so thermobaricity is necessary for a column to contain nonzero OCAPE.

3. Calculation strategy for OCAPE

Equation (4) shows that we can calculate OCAPE only if we are able to find the reference state. Again, the reference state has global minimum PE (or global minimum enthalpy) and can be reached through an adiabatic rearrangement of parcels from the current state. However, this reference state is difficult to determine because of the nonlinear EOS of seawater (Huang 2005).

Consider a statically stable ocean column, divided into M vertical layers with the same mass. Thus, we have M parcels and M vertical pressure positions defined by hydrostatic balance. We need to adiabatically rearrange the M parcels into the M vertical pressure positions to find the reference state. For realistic continuous profiles, each parcel has its own unique salinity and potential temperature, and the column has a total of $M!$ (the factorial of M) rearrangement states, among which the reference state is the one with minimum enthalpy. Note that M typically needs to be larger than 50 to ensure sufficient accuracy of the OCAPE calculation. The number of rearrangement states is so large ($M! > 3 \times 10^{64}$ even for $M = 50$) that it would be impossible for any modern computer to iterate through all of them (e.g., see Burkard et al. 2009). We therefore need to develop a more effective strategy to solve this problem.

We label the M parcels as $1, 2, \ldots, M$ and label the M vertical pressure positions as $P_1, P_2, \ldots, P_M$. For parcel i, with salinity S_i and potential temperature θ_i, its enthalpy at P_j is $h_{i,j} = h(\theta_i, S_i, P_j)$. Note again that salinity and potential temperature of a parcel are conserved under an adiabatic rearrangement. For a rearrangement state in which parcel m ($m = 1, 2, \ldots, M$) is at pressure position P_k, we can define a matrix $\mathbf{x} = [x_{i,j}]$ ($i, j = 1, \ldots, M$) that maps the current state to the rearrangement state, with $x_{m,k} = 1$ and $x_{m,l} = 0$ ($l \neq k$, $1 \leq l \leq M$) for $m = 1, 2, \ldots, M$. Thus, the column enthalpy in this rearrangement state is $\sum_{i=1}^{M}\sum_{j=1}^{M} h_{i,j}x_{i,j}$. Similarly, we can define a matrix $\mathbf{h} = [h_{i,j}](i, j = 1, \ldots, M)$. Therefore, the problem of searching for the reference state with global minimum enthalpy is to solve the following problem:

[3] In this scenario, N^2 is independent of $\rho_2(P)$ by its definition. See section 2.9.2 of Vallis (2006).

$$\text{Given an } M\times M \text{ matrix } \mathbf{h}, \text{find an } M\times M \text{ matrix } \mathbf{x} \text{ to minimize } \sum_{i=1}^{M}\sum_{j=1}^{M} h_{i,j}x_{i,j},$$
$$\text{where } \quad x_{i,j}=0 \text{ or } 1, \text{subject to } \sum_{i=1}^{M} x_{i,j}=1 \text{ for any } j, \quad \text{and} \quad \sum_{j=1}^{M} x_{i,j}=1 \text{ for any } i. \tag{6}$$

Equation (6) is easy to solve if $h_{i,j}$ is a linear function of $j(j = 1, \ldots, M)$. However, in our case it is difficult to solve (6) because enthalpy $h_{i,j}$ is a nonlinear function of pressure P_j due to thermobaricity. Fortunately, our problem (6) is actually the famous ''assignment problem'' in computational mathematics (Derigs 1985; Martello and Toth 1987; Bertsekas 1988; Martello et al. 2000; Burkard et al. 2009; Krokhmal and Pardalos 2009). This problem was effectively solved by the Hungarian algorithm (HA) with 100% accuracy (Kuhn 1955; Lawler 1976; Burkard et al. 2009). The HA is an iterative procedure that employs combinatorial optimization to find the minimum cost assignment $\sum_{i=1}^{M}\sum_{j=1}^{M} h_{i,j}x_{i,j}$. It can achieve a time complexity of $O(M^3)$, which is many orders of magnitude smaller than the $O(M!)$ time complexity of iterating through all the rearrangement states.

In summary, given profiles of potential temperature and salinity of an ocean column, we interpolate them vertically into M continuous layers with the same mass in each layer. Then we compute the $M \times M$ matrix $\mathbf{h}$ numerically using the formula for enthalpy from Feistel (2003) and solve for the reference state following the HA. Finally, we compute OCAPE using (4). In this manuscript, we use the shorthand ''HA-FullEOS'' to refer to the strategy of computing OCAPE using the HA with the full nonlinear EOS. Our algorithm takes less than 0.2 s on a personal computer with $M = 200$. The calculation converges quickly with M; for almost all the profiles, the difference between the calculated OCAPE at $M = 200$ and $M = 4000$ is less than 1%.

4. The parameter dependence of OCAPE

In this section, we elucidate the mechanism for the existence of OCAPE quantitatively and exhibit the dependence of OCAPE on key ocean parameters. In sections 4a–c, we derive analytical expressions for the OCAPE of idealized two-layer profiles (i.e., piecewise constant θ and S, one of which is CFW and the other is WSW). In section 4d, we derive approximate analytical expressions for the OCAPE of more realistic profiles with a finite thickness interface and a stably stratified WSW layer. Such analytical expressions allow OCAPE to be estimated for many real ocean profiles; since approximately two-layer profiles are frequently observed in wintertime polar oceans (see examples in section 5; Garwood et al. 1994; Akitomo 1999a; Harcourt 2005). This approach offers clearer insights as compared to the complex steps of the HA-FullEOS discussed in section 3; however, the HA-FullEOS has the advantage of being applicable to any profile of seawater. The accuracy of the analytical expressions is verified by comparison to OCAPE computed via the HA-FullEOS in sections 4d, 4e, and 5.

a. Two-layer configuration

To simplify our analysis we make the Boussinesq approximation. Since OCAPE is based on adiabatic parcel rearrangement, cabbeling has a minimal impact on OCAPE.[4] Thus, we use the following EOS that excludes cabbeling but includes thermobaricity:

$$\rho = \rho_0(1 - \alpha_\theta\delta\theta + \beta\delta S + \gamma\delta P), \tag{7}$$

where ρ_0 is the constant basic state density equal to $1030\,\mathrm{kg\,m^{-3}}$. The anomalies of potential temperature, salinity, and pressure are given by $\delta\theta$, δS, and δP, respectively; the basic states are θ_0, S_0, and P_0. The coefficients of thermal expansion, salinity contraction, and adiabatic compressibility are denoted as α_θ, β, and γ, respectively. Note that θ_0 and S_0 are constant, but α_θ, β, γ, and P_0 may depend on the vertical coordinate z. Under these approximations, Ingersoll (2005) derived the following expression for the column PE (internal energy plus gravitational energy) per unit area:

$$\frac{\mathrm{PE}}{\text{area}} = \int_{-D}^{0} (\psi_0\delta\theta + \mu_0\delta S)\rho_0\, dz + \text{constant}, \quad \text{and} \tag{8a}$$
$$\psi_0(z) = \int_{z}^{0} \alpha_\theta g\, dz', \quad \mu_0(z) = -\int_{z}^{0} \beta g\, dz'. \tag{8b}$$

[4] This is because the leading cabbeling density term $-\rho_0\gamma_{\theta\theta}\Delta\theta^2$ [e.g., see (17) of Harcourt 2005] remains approximately constant for a parcel undergoing adiabatic rearrangements. Here, $\gamma_{\theta\theta} = -1/(2\rho)(\partial^2\rho/\partial\theta^2)|_{P,S}$, which is the coefficient of cabbeling, is essentially independent of pressure: it varies by less than 10% for a pressure change from the sea level to 1500-m depth (IOC et al. 2010). The independence of OCAPE from cabbeling is verified in Fig. 3 or Table 1, which compares the OCAPE computed via the HA-FullEOS and the OCAPE computed analytically via the simplified EOS (7) that excludes cabbeling.

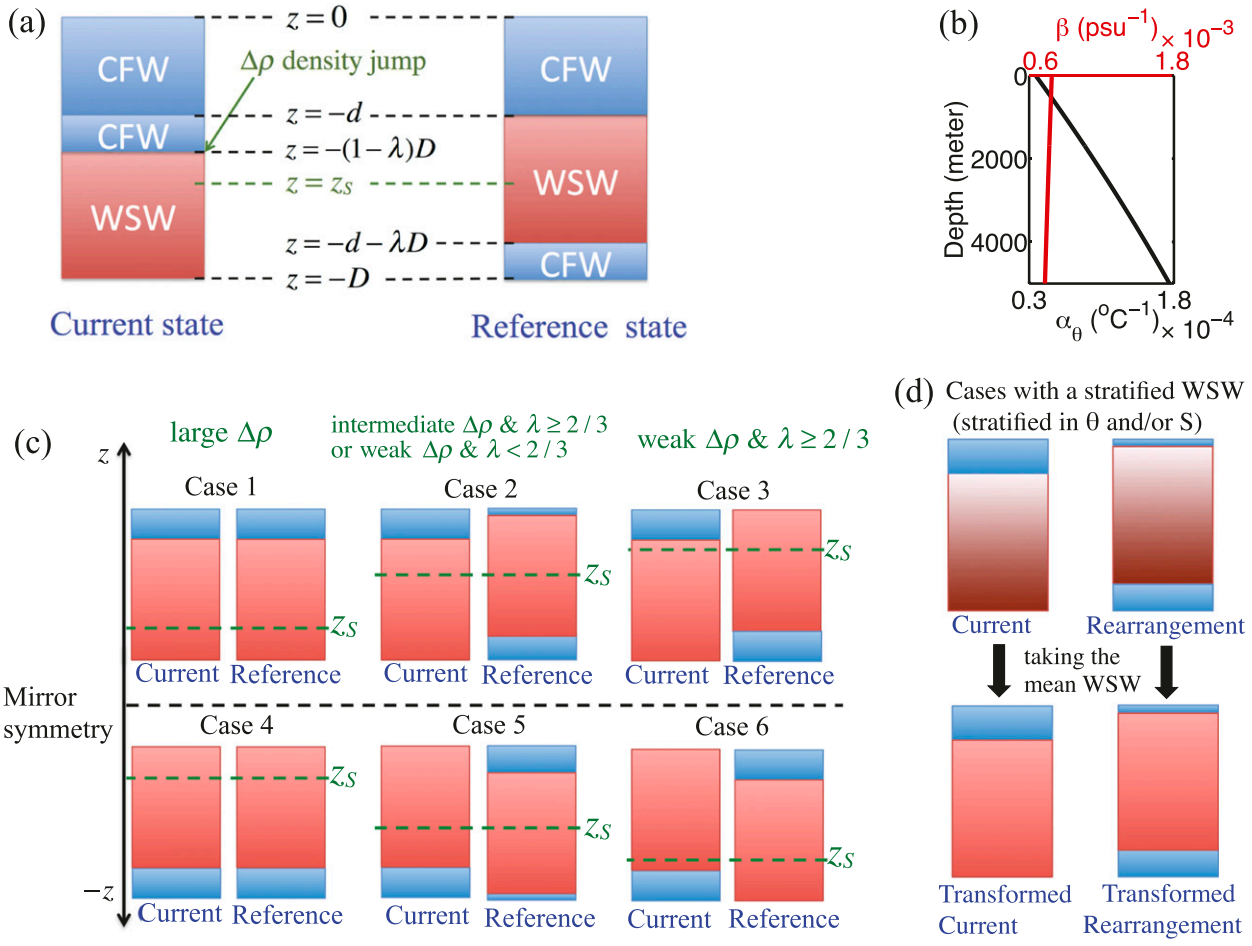

FIG. 2. (a) Schematic of the current and reference states for two-layer ocean profiles. The column depth is D, of which λD is WSW and $(1 - \lambda)D$ is CFW. There is a downward density jump $\Delta\rho \geq 0$ at the CFW–WSW interface in the current state. The densities of adiabatically repositioned CFW and WSW parcels would be equal at the critical depth $z = z_S$. We define d as the thickness of the upper CFW layer in the reference state. (b) The vertical profile of thermal expansion coefficient α_θ (black line) and saline contraction coefficient β (red line), computed from constant vertical profiles $\theta = -1$°C and $S = 34.0$ psu via the full EOS of seawater (Jackett et al. 2006). The linearity of α_θ and the independence of β on depth validate our assumptions in (10a)–(10d). (c) The current and reference states of six distinct cases, discussed in section 4. The cases are distinguished by the position of the critical depth z_S (and thus $\Delta\rho$) and λ, as described in the text. Cases 1–3 have vertical mirror symmetry to cases 4–6. (d) Schematic of the transformed current state and the transformed rearrangement state discussed in section 4d. Consider a current state that has a homogeneous CFW overlying a stratified WSW (the stratification is represented by the variation of the red color). We take the mean WSW (θ and S) to define the transformed current state. Further, we consider a rearrangement state that is statically stable (since the reference state is always statically stable). Analogously, we take the mean WSW and define a corresponding transformed rearrangement state.

Equation (8a) is essentially the Boussinesq dynamic enthalpy of the ocean column [see (13) of Young 2010] that represents the system's enthalpy (thus PE) under adiabatic conditions. Here, D is the column depth; $z = 0$ corresponds to the ocean surface, and $z = -D$ corresponds to the base of the column. The "constant" on the right-hand side of (8a) is a fixed reference PE that makes no contribution to OCAPE; only PE variations are dynamically meaningful. The symbols μ_0 and ψ_0 are the thermodynamic potentials for salinity and potential temperature, respectively.

Consider an ocean column with a homogeneous upper CFW layer ($\theta_{\rm CFW}$, $S_{\rm CFW}$) stably overlying a homogeneous lower WSW layer ($\theta_{\rm WSW}$, $S_{\rm WSW}$), as illustrated in Fig. 2a. We refer to this as the current state. The interface between the layers lies at $z = -(1 - \lambda)D$, where $0 < \lambda < 1$ represents the fraction of WSW in the whole column. We denote $\Delta\rho \geq 0$ as the downward density jump across the CFW–WSW interface. In this case, the basic state variables and their anomalies in each layer are defined as

$$\theta_0 = \frac{\theta_{\mathrm{WSW}} + \theta_{\mathrm{CFW}}}{2}, \quad S_0 = \frac{S_{\mathrm{WSW}} + S_{\mathrm{CFW}}}{2}, \tag{9a}$$

$$\delta\theta_{\mathrm{WSW}} = -\delta\theta_{\mathrm{CFW}} = \Delta\theta = \frac{\theta_{\mathrm{WSW}} - \theta_{\mathrm{CFW}}}{2}, \quad \text{and} \tag{9b}$$

$$\delta S_{\mathrm{WSW}} = -\delta S_{\mathrm{CFW}} = \Delta S = \frac{S_{\mathrm{WSW}} - S_{\mathrm{CFW}}}{2}. \tag{9c}$$

Figure 2b shows that β is almost independent of depth, while α_θ varies almost linearly with depth. For simplicity, we approximate β as a constant and α_θ as a linear function of z:

$$\alpha_\theta(z) = \alpha_0 + \alpha_z z, \tag{10a}$$

$$\alpha_0 = -\frac{1}{\rho_0}\frac{\partial\rho}{\partial\theta}\bigg|_{\theta_0,S_0,z=0}, \tag{10b}$$

$$\alpha_z = -\frac{1}{\rho_0 D}\int_{-D}^{0}\frac{\partial^2\rho}{\partial\theta\partial z}\bigg|_{\theta_0,S_0,z} dz, \quad \text{and} \tag{10c}$$

$$\beta = \frac{1}{\rho_0 D}\int_{-D}^{0}\frac{\partial\rho}{\partial S}\bigg|_{\theta_0,S_0,z} dz, \tag{10d}$$

where α_0 is the surface thermal expansion coefficient. Both α_0 and β are positive constants, while α_z is a negative constant, all of which can be computed according to the full EOS of seawater (e.g., Jackett et al. 2006). It follows from (7) and (9b)–(10d) that

$$\beta\Delta S = [\alpha_0 - (1-\lambda)D\alpha_z]\Delta\theta + \frac{\Delta\rho}{2\rho_0}. \tag{11}$$

This equation illustrates that the variation in S and θ across the CFW–WSW interface at $z = -(1-\lambda)D$, denoted as ΔS and $\Delta\theta$, respectively, produce a downward density jump $\Delta\rho$.

When $\Delta\rho > 0$, the CFW–WSW interface is stable; the WSW beneath the interface is denser than the CFW above. Consider moving a parcel of CFW down across the CFW–WSW interface and through the WSW layer adiabatically. Its density increases because of thermobaricity (see Fig. 1a) and finally equals the density of background WSW at a depth that we refer to as the critical depth $z = z_S$. Therefore, this level z_S lies below the CFW–WSW interface $z_{\mathrm{int}} = -(1-\lambda)D$. Using (7) and (9b)–(11), we obtain

$$z_S = z_{\mathrm{int}} + \frac{\Delta\rho}{2\rho_0\alpha_z\Delta\theta} = -(1-\lambda)D + \frac{\Delta\rho}{2\rho_0\alpha_z\Delta\theta}. \tag{12}$$

Parcels of CFW and WSW conserve their θ and S properties during an adiabatic parcel rearrangement. Thus, z_S is a uniquely defined depth at which the rearranged parcels of CFW and WSW have the same density, according to our simplified EOS (7).

While the CFW parcel is above the level z_S and below the CFW–WSW interface z_{int}, it is positively buoyant, and this region represents an energy barrier; thus, extra energy is required to make the parcel sink. Below the critical depth z_S, the parcel experiences a negative buoyancy force, and potential energy is released as it sinks. Horizontal convergence caused by wind forcing may be responsible for deepening a well-mixed layer of CFW to this critical depth z_S and therefore triggering convection, as is the case in deep lakes (Weiss et al. 1991; Akitomo et al. 1995; Schmid et al. 2008).

b. *Analytical expressions for OCAPE in two-layer profiles*

Conceptually, we have the following three cases for OCAPE:

(i) If z_S lies at the midplane of the WSW layer, the energy input (required to move a CFW parcel from the upper boundary of the WSW layer to z_S) is approximately equal to the energy release (from moving the same CFW parcel from z_S to the bottom of the WSW layer). This equality is because of the nearly linear dependence of α_θ on depth (see details in section 4c). If z_S lies below the midplane of the WSW layer, the energy input to the fluid in crossing the barrier is greater than the energy released once the barrier is crossed. In both scenarios moving CFW downward cannot produce a lower energy state. Thus, the current state is the reference state and OCAPE = 0. We refer to this as case 1 and illustrate it in Fig. 2c.

(ii) When z_S lies above the midplane of the WSW layer in the current state, the energy required to move a CFW parcel from the upper boundary of the WSW layer to $z = z_S$ is smaller than the energy released when the parcel descends from $z = z_S$ to the bottom of the WSW layer. Thus, moving CFW to the bottom of the WSW layer leads to a lower column PE (i.e., OCAPE > 0). This process also raises the midplane of the WSW. Eventually the midplane will coincide with the level z_S, and then moving more CFW to the bottom of the WSW layer can no longer lead to a lower column PE, as in case 1 above. This is the reference state for case 2, in which a portion of the CFW lies above the WSW layer and a portion lies below the WSW layer.

(iii) Case 3 occurs when moving all of the CFW below the WSW layer still does not raise the midplane of the WSW layer as high as the level z_S. This state is the reference state. For similar reasons to case 2 above, OCAPE is positive for case 3.

We now analytically derive the reference state and OCAPE for these three cases.

The reference (minimum PE) state, by definition, has zero OCAPE and is statically stable to infinitesimal perturbations. Consider moving CFW and WSW parcels adiabatically to the same level z. According to the definition of z_S, CFW is less dense than WSW if $z > z_S$, is as dense as WSW if $z = z_S$, and is denser than WSW if $z < z_S$. Therefore, for the reference state to be statically stable, it must have CFW above WSW for $z \geq z_S$ and CFW beneath WSW for $z < z_S$ (Fig. 2a). Therefore, the WSW–CFW interface $z = -d - \lambda D$ in the reference state has to lie beneath $z = z_S$, where d is the thickness of the upper layer of CFW in the reference state (Fig. 2a). Thus, the lower bound of d is $(-z_S - \lambda D)$. The upper bound of d is the total thickness of CFW [i.e., $(1-\lambda)D$]. Therefore, given a current state with parameters D, z_S, and λ $(0 < \lambda < 1)$, the possible reference states are

$$\begin{aligned} &\text{CFW at:} \quad -d < z < 0, \ -D < z < -d - \lambda D, \\ &\text{WSW at:} \quad -d - \lambda D < z < -d, \\ &\text{with } \max(0, -z_S - \lambda D) \leq d \leq (1-\lambda)D. \end{aligned} \tag{13}$$

Here, d is a variable; the reference state by definition corresponds to a d that globally minimizes the PE of the state (13), where

$$\frac{\text{PE}}{\text{area}} = -\rho_0 g \alpha_z \Delta\theta \lambda D \left[d^2 + 2\left(z_S + \frac{1}{2}\lambda D \right) d \right] + \text{constant}. \tag{14}$$

This can be derived by evaluating the integral on the right-hand side of (8a). The constant on the right-hand side of (14) again makes no contribution to the OCAPE.

Every possible reference state belongs to one of three cases, distinguished by whether no CFW (case 1), a fraction of the CFW (case 2), or all of the CFW (case 3) moves beneath the WSW. These cases are determined by solving d that minimizes PE given by (14). These cases are detailed individually below.

1) CASE 1

For stratification $\Delta\rho$ sufficiently large that z_S lies beneath the center of the WSW,

$$z_S \leq -(1 - \lambda/2)D, \quad \text{i.e. } \Delta\rho \geq -\rho_0 \alpha_z \Delta\theta \lambda D, \tag{15a}$$

the reference state is simply the current state (Fig. 2c), that is, (13) with

$$d = (1-\lambda)D, \tag{15b}$$

and therefore the column contains no OCAPE:

$$\text{OCAPE} = 0. \tag{15c}$$

2) CASE 2

For sufficiently weak stratification $\Delta\rho$ such that z_S lies above the center of the WSW and deeper than half the WSW layer thickness,

$$\begin{aligned} &-(1-\lambda/2)D < z_S < -(\lambda/2)D, \\ &\text{i.e. } -\rho_0 \alpha_z \Delta\theta \lambda D > \Delta\rho \geq -\rho_0 \alpha_z \Delta\theta (3\lambda - 2) D, \end{aligned} \tag{16a}$$

the reference state is (13) with

$$d = \left(1 - \frac{3}{2}\lambda\right) D - \frac{\Delta\rho}{2\rho_0 \alpha_z \Delta\theta} = -z_S - \frac{1}{2}\lambda D. \tag{16b}$$

In this case, a portion of the CFW moves below the WSW, leaving the WSW exactly centered around $z = z_S$ to reach the reference state (Fig. 2c), and

$$\text{OCAPE} = -g\alpha_z \Delta\theta D^2 \left[\frac{1}{4}\lambda \left(\lambda + \frac{\Delta\rho}{D\rho_0 \alpha_z \Delta\theta} \right)^2 \right]. \tag{16c}$$

Here, OCAPE is column averaged, with dimensions of energy/mass.

3) CASE 3

For only $\lambda \geq 2/3$ and sufficiently weak stratification $\Delta\rho$, such that both the level $z = z_S$ and the CFW–WSW interface lie no deeper than half the WSW thickness,

$$\begin{aligned} &z_S \geq -(\lambda/2)D, -(1-\lambda)D \geq -(\lambda/2)D, \\ &\text{i.e. } -\rho_0 \alpha_z \Delta\theta (3\lambda - 2) D > \Delta\rho \geq 0, \end{aligned} \tag{17a}$$

and then the reference state is (13) with

$$d = 0. \tag{17b}$$

Thus, in this case all of the CFW moves below the WSW to reach the reference state (Fig. 2c), and OCAPE (column averaged, with dimensions of energy/mass) is

$$\text{OCAPE} = -g\alpha_z \Delta\theta D^2 \left\{ \lambda(\lambda - 1) \left[(1 - 2\lambda) - \frac{\Delta\rho}{D\rho_0 \alpha_z \Delta\theta} \right] \right\}. \tag{17c}$$

Type II convection can also occur in a two-layer profile with WSW overlying CFW. This type of convection has not yet been observed, but in principle it could occur in the real ocean (see discussion in section 6). In this scenario, following similar derivations as above, we find that there are still three cases, denoted as cases 4, 5, and 6. They have mirror symmetry in the vertical (including the critical depth z_S) with cases 1, 2, and 3, respectively, as shown in

Fig. 2c. The analytical expressions for their OCAPE are therefore also identical (for cases 4–6, d should denote the bottom CFW thickness in the reference state; $\Delta\rho$ is still the positive downward density jump across the interface in the current state). Note again that the PE release is always associated with moving CFW through the WSW vertically and never the reverse (see Fig. 1).

c. *Alternative explanation for the threshold of cases 1–3*

Here, we explain the thresholds of $\Delta\rho$ (or z_S) of cases 1–3 from the viewpoint of a single parcel rearrangement, similar as points i–iii in section 4b but using a quantitative approach. We begin from a hypothetical state in which a thickness Δz of CFW has already been displaced adiabatically from the CFW–WSW interface $z = z_{\rm int}$ to the bottom $z = z_{\rm bot}$. Now consider moving a single CFW parcel adiabatically from the new upper CFW–WSW interface $z_{\rm int} + \Delta z$ to the lower WSW–CFW interface $z_{\rm bot} + \Delta z$. The associated change in the column's PE ΔPE is equal to the change of column's enthalpy ΔH, as in section 2. The entropy and salinity of this parcel remain unchanged. Via a derivation similar to that of (A.5) of Adkins et al. (2005), we obtain an expression for ΔH as follows:

$$\Delta \mathrm{PE} = \Delta H = \frac{mg}{\rho_0}\int_{z_{\rm int}+\Delta z}^{z_{\rm bot}+\Delta z} \rho'(z)\,dz, \tag{18a}$$

$$z_{\rm int} = -(1-\lambda)D, \quad z_{\rm bot} = -D, \quad \text{and} \tag{18b}$$

$$\rho'(z_{\rm int}) = -\Delta\rho, \quad \rho'(z_S) = 0, \quad \frac{\partial \rho'}{\partial z} = \text{constant}. \tag{18c}$$

Here, m is the mass of this moving parcel, and $\rho'(z)$ is the density anomaly of this parcel with respect to the ambient WSW, which depends linearly on z since α_θ varies linearly with z.

This parcel rearrangement can be considered a two-step process. The first step is the displacement from $z_{\rm int} + \Delta z$ to z_S, which requires external work input to overcome buoyancy resistance ($\rho' < 0$). The second step is the displacement from z_S to $z_{\rm bot} + \Delta z$, which releases PE (i.e., decreases ΔPE) because ρ' is positive throughout these depths (due to thermobaricity). If the PE released in the second step is larger than the external work input in the first step, then ΔPE is negative and this column contains OCAPE. Since $\rho'(z)$ is linear with depth, this situation occurs only if $z_S > z_c$, according to (18a) and (18c). Here, z_c is the depth of the center of the two new interfaces:

$$\begin{aligned} z_c &= 0.5[(z_{\rm int}+\Delta z) + (z_{\rm bot}+\Delta z)] = -(1-0.5\lambda)D + \Delta z,\\ &\text{where} \quad -(1-0.5\lambda)D \le z_c \le -0.5\lambda D,\\ &\text{since} \quad 0 \le \Delta z \le (1-\lambda)D. \end{aligned} \tag{19}$$

Therefore, there are three categories for the initial OCAPE, which are determined by z_S. (i) When $z_S \le -(1 - 0.5\lambda)D$, this ensures $z_S \le z_c$ for any Δz according to (19). Thus, the initial column contains no OCAPE; this corresponds to case 1. (ii) When $-(1 - 0.5\lambda)D < z_S \le -0.5\lambda D$, there exists a range of Δz such that $z_S > z_c$. Therefore, the initial column contains OCAPE, and the reference state corresponds to the value of Δz that makes $z_S = z_c$. This is case 2. (iii) When $-0.5\lambda D < z_S$, the condition $z_S < z_c$ is satisfied for any Δz. Therefore, the initial column contains OCAPE, and the reference state corresponds to $\Delta z = (1 - \lambda)D$ (i.e., all of the CFW moves beneath the WSW). This is case 3.

d. *Analytical expressions for OCAPE of more realistic profiles: With stably stratified WSW*

We now derive analytical expressions for the OCAPE in somewhat more realistic water column profiles. The profiles still have two layers, as above, but we consider a CFW–WSW interface of finite thickness and introduce a constant positive stratification in the WSW layer. Harcourt (2005) pointed out that realistic CFW–WSW transitions have finite vertical extent due to mixed layer entrainment or shear, which can significantly impact the dynamics by inducing cabbeling instability. However, the thickness of this interface is still much thinner than the ocean column under consideration [about 20–100 vs 1000 m; see realistic profiles in section 5 and also Harcourt (2005)]. It therefore minimally impacts the OCAPE value (<10% in our tests), since the OCAPE is defined by adiabatic rearrangements of water parcels throughout the entire column parcels. We verify this later in Table 1.

To estimate the OCAPE for this configuration we modify the two-layer current state discussed in the previous sections: the current state now not only has a stable density jump $\Delta\rho$ across the CFW–WSW interface, but also has a linearly stratified WSW layer with positive buoyancy frequency $N^2_{\rm wsw}$ (see examples in Table 1). To a good approximation, our analytical expressions for the OCAPE (15a)–(17c) still apply, except that $\Delta\rho$ must be replaced by $\delta\rho$ throughout, where $\delta\rho$ is as the density change from the bottom of the CFW to the middepth of the WSW:

TABLE 1. OCAPE by analytical expressions derived in section 4d vs the OCAPE computed via the HA-FullEOS described in section 3. The latter uses the exact water column stratification described below, whereas the former neglects the finite thickness interface between the CFW and WSW (assumed to be CFW instead). These two methods differ by less than ~10% in all eight examples. All examples have a column depth of 1000 m and a homogeneous CFW ($\theta = -1.6$°C and $S = 34.47$ psu) overlying a stratified WSW layer that has a constant positive buoyancy frequency $N^2_{\rm wsw}$. The λ is the fraction of the WSW in the whole column, $\Delta\rho$ is the downward density jump across the CFW–WSW interface, and $\delta\rho$ is the density change from the bottom of the CFW to the middepth of the WSW [defined in (20)]. Examples 1–4 have a WSW of constant $\theta = 0.9$°C, with a S stratification (which can be determined from $\Delta\rho$, $N^2_{\rm wsw}$, the S of the CFW, and the column's θ profile). Examples 5–8 have a WSW of constant $S = 34.65$ psu, with a θ stratification (similarly determinable as above). Within the finite thickness CFW–WSW interface, the θ and S properties vary linearly with depth. The classification into cases 1–3 follows section 4b.

Example No.	1	2	3	4	5	6	7	8
λ	0.7	0.7	0.9	0.9	0.7	0.7	0.9	0.9
Interface thickness (m)	0	0	40	40	40	40	40	40
$\Delta\rho$ (kg m^{-3})	5×10^{-3}	3×10^{-3}	4×10^{-3}	5×10^{-3}	5×10^{-3}	4×10^{-3}	1×10^{-3}	6×10^{-3}
$N^2_{\rm wsw}$(s^{-2})	6×10^{-7}	1×10^{-7}	4×10^{-7}	5×10^{-7}	2×10^{-7}	1×10^{-7}	4×10^{-7}	3×10^{-7}
$\delta\rho$ (kg m^{-3})	2.7×10^{-2}	6.7×10^{-3}	2.2×10^{-2}	2.8×10^{-2}	1.2×10^{-2}	7.4×10^{-3}	1.9×10^{-2}	2.0×10^{-2}
Classification	Case 1	Case 2	Case 3	Case 2	Case 2	Case 2	Case 3	Case 3
OCAPE, analytical (J kg^{-1})	0	1.8×10^{-2}	7.2×10^{-3}	2.6×10^{-3}	8.1×10^{-3}	1.5×10^{-2}	1.0×10^{-2}	0.9×10^{-2}
OCAPE, HA-FullEOS (J kg^{-1})	0	1.7×10^{-2}	7.5×10^{-3}	2.5×10^{-3}	7.7×10^{-3}	1.4×10^{-2}	1.1×10^{-2}	1.0×10^{-2}

$$\delta\rho = \Delta\rho + \frac{\rho_0}{2g}\int_{-D}^{-(1-\lambda)D} N^2_{\rm wsw}\, dz, \qquad (20)$$

where $-D$ and $-(1-\lambda)D$ are again, respectively, the depths of the lower and upper boundary of the WSW layer in the current state. We define a "transformed current state," which is identical to the current state except that the WSW layer is replaced with a homogeneous layer having the depth-averaged WSW properties of the current state (Fig. 2d). By definition, $N^2_{\rm wsw}$ is zero in the transformed current state, and the downward density jump across the interface is approximately $\delta\rho$, defined in (20). Recall that any rearrangement state is attainable via adiabatic vertical parcel rearrangements from the current state. We only consider those rearrangement states that are potentially the reference state: they always have the denser WSW lying beneath the less dense WSW, since the reference (minimum PE) state should be statically stable. Similarly we can define a "transformed rearrangement state," which is the same as the rearrangement state except that its WSW layer(s) should be again replaced by the mean WSW (Fig. 2d). Thus, this transformed rearrangement state is a rearrangement state from the transformed current state. The key point is that the PE difference between the current state and the rearrangement state is well approximated by the PE difference between the transformed current state and the transformed rearrangement state.[5] This PE difference is exactly the OCAPE when the rearrangement state is the reference state. Therefore, the current state has approximately the same OCAPE as the corresponding transformed current state, whose OCAPE can be computed analytically from (15a) to (17c) (using $\delta\rho$ to replace $\Delta\rho$). Note that $N^2_{\rm WSW}$ has an upper bound, above which the water column contains zero OCAPE [from (20) the upper bound of $N^2_{\rm WSW}$ is determined by the upper bound of $\delta\rho$ stated in (16a) and (17a), where we again should use $\delta\rho$ to replace $\Delta\rho$]. This upper bound of $N^2_{\rm WSW}$ ensures that the reference state, as estimated by the OCAPE calculation strategy above, is always statically stable at its CFW–WSW and WSW–CFW interfaces (by following the arguments ii and iii in the beginning of section 4b).

This is verified by the eight examples in Table 1, which show agreement between the OCAPE estimated analytically and the OCAPE computed via the HA-FullEOS (see also section 5 for further verification using realistic profiles). Note that the OCAPE computed via the HA-FullEOS uses the exact water column stratification described in Table 1, whereas our analytical estimate neglects the finite thickness interface between the CFW and WSW, as described above.

e. Implications

Equations (15a)–(17c) provide thorough information about the parameter dependence of OCAPE in a two-layer profile, which is uniquely determined by the following five parameters: α_z, $\Delta\theta$, D, λ, and $\Delta\rho$ (or, more generally, $\delta\rho$). The sensitivity of OCAPE to these five parameters is plotted in Figs. 3a–e, respectively. The dashed black lines in Figs. 3a–d have been computed using the HA-FullEOS in section 3. The solid black lines in Figs. 3a–d and the colored lines in Fig. 3e have been

[5] In other words, the PE difference between the current state and the transformed current state is well approximated by the PE difference between the rearrangement state and the transformed rearrangement state. This PE difference is approximately equal to the change of the system's gravitational energy when the stratified WSW is replaced by the mean WSW (Fig. 2d).

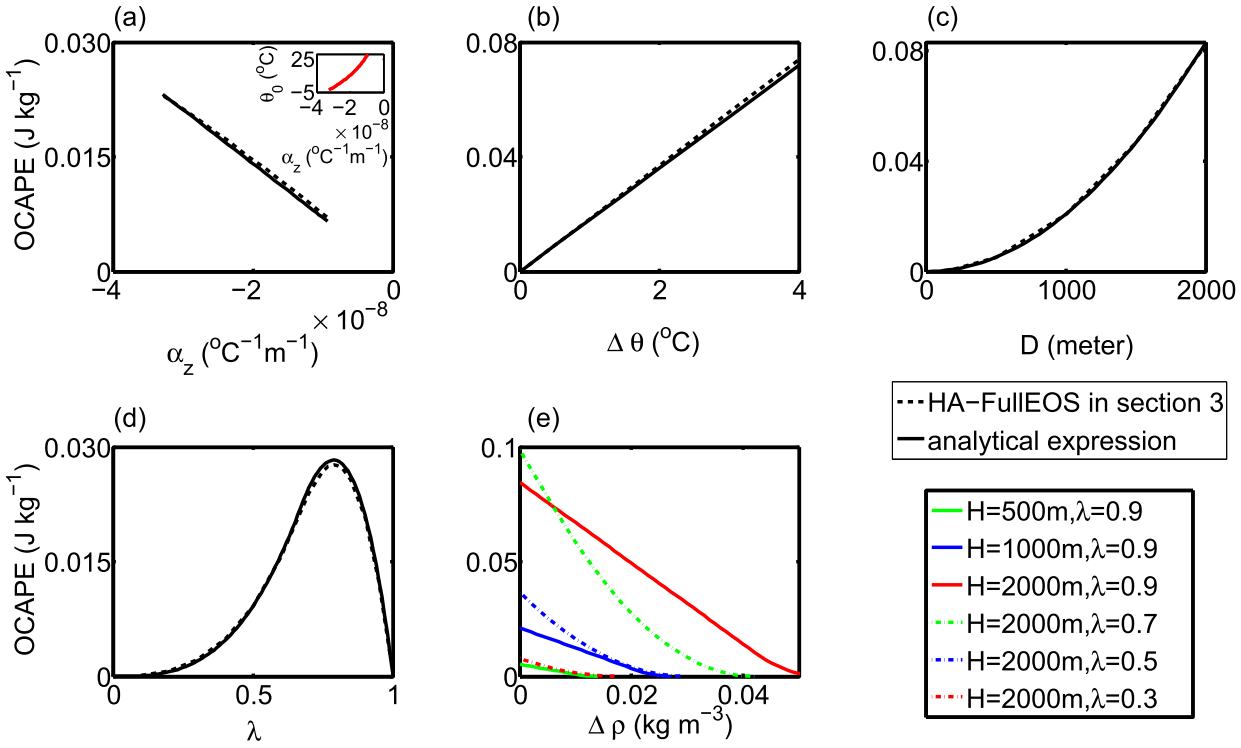

FIG. 3. Parameter dependence of OCAPE, as discussed in section 4e. The dashed black lines in (a)–(d) have been computed using the HA-FullEOS in section 3. The solid black lines in (a)–(d) and the colored lines in (e) have been computed using analytical expressions in section 4. These are for two-layer profiles with CFW overlying WSW. Here, α_z is the derivative of thermal expansion coefficient with respect to vertical coordinate; $\Delta\theta$ is half of the difference of potential temperature between the CFW and the WSW; D is the ocean column depth; λ is the fraction of the WSW in the whole column; and $\Delta\rho$ is the downward density jump across the CFW–WSW interface. (a) Sensitivity to α_z, with fixed $\Delta\theta = 1°C$, $D = 1000\,m$, $\lambda = 9/10$, and $\Delta\rho = 0$. The inset shows the sensitivity of α_z to potential temperature θ_0, computed via (10c) using the full EOS of seawater (Jackett et al. 2006) with fixed $S_0 = 34.0$ psu and $D = 1000\,m$. (b) Sensitivity to $\Delta\theta$, with fixed $\alpha_z = -2.4 \times 10^{-8}\,°C^{-1}\,m^{-1}$ ($\theta_0 = 4°C$) and the same D, λ, and $\Delta\rho$ as (a). (c) Sensitivity to D, with fixed $\alpha_z = -3.0 \times 10^{-8}\,°C^{-1}\,m^{-1}$ ($\theta_0 = 0°C$) and the same $\Delta\theta$, λ, and $\Delta\rho$ as (a). (d) Sensitivity to λ, with the same α_z as (c) and the same $\Delta\theta$, D, and $\Delta\rho$ as (a). (e) Sensitivity to $\Delta\rho$ for different D and λ, with the same α_z and $\Delta\theta$ as (c).

computed using the analytical expressions in section 4b. The strong agreement of these methods (differing by less than 2%) confirms the accuracy of our analytical approach.

As shown in Fig. 3a, OCAPE is linearly proportional to α_z, which is defined by (10c) and represents the strength of thermobaricity. We found that α_z is essentially independent of S_0 and D (not shown), but it is sensitive to θ_0 (the mean θ of the CFW and WSW). This is illustrated in the inset in Fig. 3a, in which we have computed α_z using fixed $S_0 = 34.0$ psu and $D = 1000\,m$ and the full EOS for seawater (Jackett et al. 2006). Therefore, the polar oceans may contain more OCAPE because of the larger magnitude of α_z at lower temperatures. This may partially explain less frequent observations of thermobaric convection at lower latitudes (e.g., see the summary of observations in the modeling studies of Akitomo 1999a,b). In wintertime polar oceans, θ_0 is approximately in the range of −2° to 4°C (Garwood et al. 1994; McPhee 2000; Wadhams et al. 2002), so α_z is approximately a constant $\sim -3 \times 10^{-8}\,°C^{-1}m^{-1}$.

Figure 3b shows that OCAPE is linearly proportional to the potential temperature contrast between CFW and WSW (i.e., $2\Delta\theta$), which is required for thermobaric instability. In the winter Weddell Sea, $\Delta\theta$ is approximately 0.5°–2°C (Gordon 1991; Gordon and Huber 1995; McPhee 2003).

OCAPE depends quadratically on the column depth D, as shown in Fig. 3c. This quadratic dependence occurs because the vertical distance that CFW must move to reach the reference state and the thermobarically induced density change of the adiabatically transported CFW both increase linearly with D. The most dynamically relevant D is the maximum depth of convection, which we propose a strategy to predict in Part II.

OCAPE depends strongly on λ, the WSW fraction in the whole column (Fig. 3d). Different WSW fractions may result in qualitatively different reference states and

thus different OCAPE (e.g., case 3 requires $\lambda \geq 2/3$ as in section 4b). When λ equals 0 or 1, OCAPE is zero, as there is no temperature variation. OCAPE has a maximum at $\lambda \sim 0.8$ for profiles with zero stratification (Fig. 3d).

The downward density jump across the interface $\Delta\rho$ may have values between 0 and 0.1 kg m^{-3} in the winter Weddell Sea (McPhee 2000, 2003). Figure 3e shows that $\Delta\rho$ can significantly impact OCAPE within this range. This dependence is quadratic for case 2 and linear for case 3. The dashed blue line and the dashed red line both suggest the transition from case 1 to case 2 with a decreasing $\Delta\rho$ but never reach case 3, since $\lambda < 2/3$. All other curves have $\lambda > 2/3$ and therefore suggest the transition from case 1 to case 2 and then from case 2 to case 3 with a decreasing $\Delta\rho$. OCAPE is always positive for $\Delta\rho = 0$.

Given the parameter space, Fig. 3 produces a rough estimate for the magnitude of OCAPE in wintertime polar oceans, which is about 0–0.05 J kg^{-1}. The release of this OCAPE can induce convection with vertical velocities of ~0–10 cm s^{-1}, using a 10% release fraction[6] (see Part II for detailed discussions). This value might partly contribute to the observed strong deep convection of ~7–10 cm s^{-1} in polar oceans (Schott et al. 1993; Marshall and Schott 1999).

5. OCAPE in the winter Weddell Sea

We estimate OCAPE in profiles from wintertime observations in the Weddell Sea. A characteristic feature of the Weddell Sea water masses is the warm (~0–1°C) and salty deep water (Circumpolar Deep Water) found immediately beneath the pycnocline at 100- to 200-m depth, especially around Maud Rise, known as the ''warm pool'' (Gordon and Huber 1995; De Steur et al. 2007). During winter, nearly the entire extent of the Weddell Sea is covered by sea ice due to strong surface cooling, and the mixed layer is close to the freezing point ~−1.9°C (Parkinson and Cavalieri 2012; Renfrew et al. 2002). This gives rise to an approximately two-layer stratification (CFW overlying WSW) that is frequently observed (Gordon and Huber 1990; McPhee 2003; Harcourt 2005).

Figure 4a shows one such two-layer observation (McPhee et al. 1996), in which the water column properties were measured down to ~1500-m depth. The CFW–WSW interface is located between depths of ~180 and ~200 m. The finite thickness of this interface, as opposed to a discontinuous jump, is due to mixed layer entrainment or shear and is key to inducing cabbeling instability (Harcourt 2005). The OCAPE of this profile is displayed in Fig. 4b as a function of depth (i.e., the OCAPE for the part of the ocean between the surface and the specified depth) and has been calculated using both the HA-FullEOS from section 3 and the analytical method described in section 4d. For the analytical method, λ is estimated based on an interface depth of 190 m; $\Delta\theta$ is estimated using (9b) based on the mean properties of the CFW (above 180-m depth) and the mean of the WSW (beneath 200-m depth); $\delta\rho$ is estimated using (20). Similar to Fig. 3c, OCAPE has a quadratic dependence on the depth [see (16c) and (17c)]. OCAPE is approximately zero between depths of 0–700 m and increases to 0.009 J kg^{-1} at 1500-m depth. For an actual convection event, the OCAPE based on the maximum depth of convection (~1000 m for this case) is most dynamically relevant. In Part II, we propose to evaluate the maximum depth of convection from an energetic perspective.

The OCAPE of a profile can be significantly modified because of wintertime surface buoyancy forcing. The profiles of Fig. 4a come from sea ice–covered regions, and we assume a sea ice production rate of 1.5 cm day^{-1} (1–1.5 cm day^{-1} is common for the winter Weddell Sea; see Harcourt 2005; Lange et al. 1989). Therefore, CFW remains at the freezing point but becomes saltier by brine rejection; thus, the interface between the mixed layer and the WSW beneath becomes less stably stratified (i.e., $\Delta\rho$ decreases), which leads to increased OCAPE. Here, we estimate the increase of OCAPE based on the profiles of Fig. 4a, except with a homogeneously saltier mixed layer following sea ice production. This is rather a scaling analysis and the assumption is idealized (see similar assumptions applied in Garwood et al. 1994; Årthun et al. 2013): In reality, cabbeling instability at the interface could induce type III convection before $\Delta\rho$ is completely eroded (Harcourt 2005), resulting in the shoaling of the mixed layer and also the partial release of OCAPE (see simulation in Part II). Our result is shown in Fig. 4c for the column depth of 1000 m (the maximum depth of convection); 4.5 days' ice formation reduces $\Delta\rho$ to approximately zero and increases the OCAPE from ~0.001 to ~0.01 J kg^{-1}. Figure 4c resembles Fig. 3e and is determined by the dependence of OCAPE on $\Delta\rho$, which is quadratic for $\Delta\rho$ of moderate strength [case 2; see (2)] and becomes linear for smaller $\Delta\rho$ [case 3; see (17c)].

In Fig. 4d, we show another approximately two-layer profile from observations (McPhee et al. 1996). In this case, the dependence of the OCAPE on the column

[6] That is, $(2 \times 0.05\,\text{J kg}^{-1} \times 10\%)^{0.5} = 0.1\,\text{m s}^{-1}$ according to KE = 0.5 × mass × velocity^2.

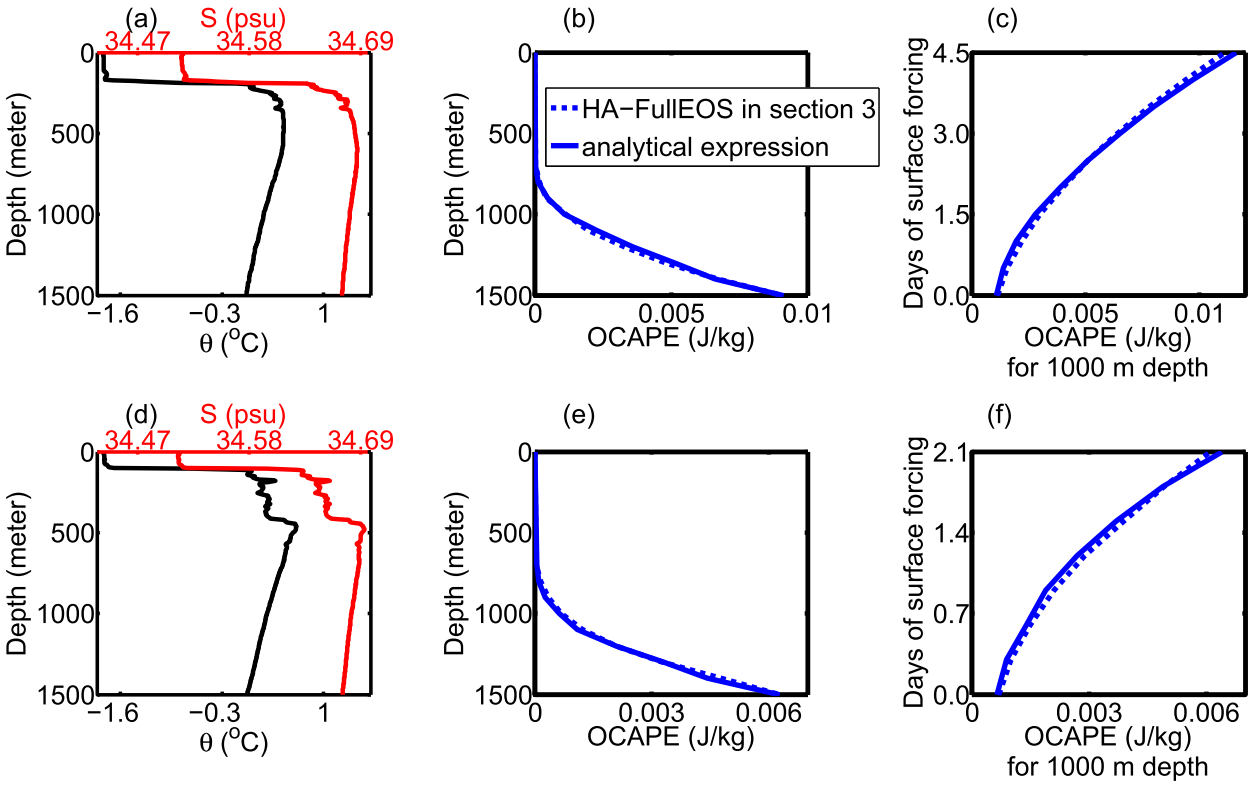

FIG. 4. (a) Profiles of potential temperature θ and salinity S from the wintertime Weddell Sea, obtained from Maud Rise (65.4605°S, 2.4007°E) on 2 Aug 1994, Antarctic Zone Flux Experiment (ANZFLUX) CTD profile station 48 (courtesy of Bruce Huber; McPhee et al. 1996). (b) OCAPE vs depth of the profiles shown in (a); at each depth we computed the OCAPE, assuming that depth to be the bottom of the ocean (i.e., not permitting any adiabatic rearrangement of the fluid below that depth). The dashed and solid blue lines are from the HA-FullEOS in section 3 and the analytical solution derived from section 4d, respectively (see section 5 for details). (c) Estimated temporal evolution of OCAPE for 1000-m depth of profiles in (a) during a winter surface brine rejection forcing. This forcing equals an ice formation rate of 1.5 cm day^{-1}, which is common for the winter Weddell Sea (Harcourt 2005; Lange et al. 1989). Calculation methods are described in the text of section 5. (d),(e),(f) As in (a)–(c), but for profiles observed over Maud Rise (65.5177°S, 1.1315°E) on 1 Aug 1994, ANZFLUX CTD profile station 46; 1500 m is approximately the maximum depth of measurement for profiles in both (a) and (d). Panels (b),(c),(e), and (f) share the same legend.

depth (Fig. 4e) and on the surface buoyancy forcing (Fig. 4f) is similar to the previous example (Figs. 4b,c). There is a difference ($\leq$35%) between their OCAPE values for the same parameters (the column depth and the days of surface forcing). This is mainly due to the differing thickness of CFW and also the stratification N^2 of the WSW layer. In all of these examples, the OCAPE calculated via the HA-FullEOS and our analytical expressions agree well with each other (differing by less than 15%).

6. Discussion and conclusions

a. *Key results*

We summarize our key results as follows:

(i) We develop the concept of OCAPE to evaluate the contribution of thermobaricity to the KE of type II and type III ocean convection. OCAPE parallels convective available potential energy (CAPE), a key energy source for atmospheric moist convection that has long been used to forecast moist convection. Both OCAPE and CAPE measure the upper limit of stored PE in a fluid column that can be released under adiabatic vertical parcel rearrangements.

(ii) OCAPE can also be conceptually compared to available potential energy (APE), a major energy source for ocean mesoscale geostrophic turbulence. OCAPE arises from thermobaricity, while APE arises mainly from baroclinicity. OCAPE is due to vertical rearrangement of parcels, while APE requires both vertical and lateral rearrangement of parcels. Both OCAPE and APE are based on adiabatic parcel rearrangements.[7]

[7] For APE, see section 2b of Huang (2005), section 3 of Winters et al. (1995), and Vallis (2006).

(iii) We propose an innovative strategy, the HA-FullEOS, to accurately solve the global minimum PE state of an ocean column and thus determine OCAPE for any ocean column profile (section 3).

(iv) For approximately two-layer profiles, which are widely observed in wintertime polar oceans, we derive an analytical solution for OCAPE. This illustrates the dependence of OCAPE on key parameters in the real ocean such as the column depth and the density stratification (Fig. 3). We quantitatively classify OCAPE into three different cases (section 4b).

(v) We find an OCAPE $\sim$0.001–0.01 J kg^{-1} from hydrographic profiles from the wintertime Weddell Sea. Wintertime surface buoyancy loss may significantly enhance OCAPE (e.g., by $\sim$0.01 J kg^{-1}; Fig. 4). This OCAPE of 0.01 J kg^{-1}, if totally released into KE, would induce a significant vertical velocity of $\sim$14 cm s^{-1} and hence cause strong vertical tracer transports and mixings.

b. Limitations

OCAPE is a quantitative concept that evaluates the contribution of KE due to thermobaricity in type II and type III convection. OCAPE, like APE and CAPE, is defined based on adiabatic parcel rearrangements. As a result, it excludes the effects of diabatic processes. It also excludes cabbeling, since cabbeling essentially contributes nothing to the density change of a parcel under adiabatic rearrangements (see footnote 4 for details). However, cabbeling and diabatic processes, like thermobaricity, are also key factors that modulate type II and type III convection (Harcourt 2005; Akitomo 2011). In Part II, we investigate their associated contributions to the KE budget of type II and type III convection. We also investigate the dynamics of the conversion of OCAPE to KE that is not included in this paper.

c. Discussion

Hoppema et al. (2006) have observed frequent and precipitous warming events (sometimes up to 1°C warming) at 91-m depth in Maud Rise occurring in late winter and early spring (the same region and timing of our Weddell Sea profiles in Fig. 4). We will investigate the possible contribution of the release of OCAPE to these warming events in a subsequent study. Indeed, Maud Rise has a semipermanent two-layer stratification (e.g., see Fig. 8 of De Steur et al. 2007) that could easily accumulate OCAPE during the winter. The release of OCAPE may also impact the dynamics of the Weddell Gyre through strong vertical mixing [e.g., see Su et al. (2014) for the related dynamics]. OCAPE may exist in the Greenland Sea and may contribute to the formation of North Atlantic Deep Water (NADW) by deep convection. The potential role of OCAPE in other deep convection sites, such as the Ross, Labrador, and Mediterranean Seas, requires further evaluation. Especially in the Ross Sea, an important region for the production of AABW, two-layer stratification with CFW overlying WSW has been frequently observed over the western continental slope (see Fig. 2 of Gordon et al. 2009). For the Arctic deep water at the Canada basin (below 2.7-km depth), a recent study by Carmack et al. (2012) proposes that thermobaric instability might effectively transfer geothermal heat upward. They have observed CFW overlying WSW (see their Figs. 2 and 3), which indicates the potential existence of OCAPE in the Arctic Ocean.

Our theory demonstrates that OCAPE can also exist when WSW lies above CFW (Fig. 2c, cases 5–6). A potential instance is the two-layer stratification in the winter Japan Sea (see Fig. 6 of Talley et al. 2004). Talley et al. (2003) observe Japan Sea deep convection in late winter 2000 and 2001. They find that the strong surface cooling densifies the warm salty surface water (about 0.6 to 1.6°C) outside the ice-covered area until it finally becomes as dense as or denser than the cold freshwater beneath (about 0°C); see Fig. 3 of Talley et al. 2003). This nearly neutrally stratified two-layer profile may contain positive OCAPE according to our theory in section 4. Thus, OCAPE might contribute to the observed convection events down to 1.5-km depth. We plan to investigate this in a separate study.

In the Last Glacial Maximum (LGM), the Atlantic Ocean had highly stable stratification, with cold, salty AABW lying beneath cold, fresh NADW (Labeyrie et al. 1992). However, Adkins et al. (2005) argue that geothermal heating for thousands of years might warm the AABW by a few degrees and thus charge the thermobaric capacitor (i.e., in our terminology, accumulate OCAPE). They further propose that the induced thermobaric instability might partly account for the observed global Dansgaard/Oeschger events, the abrupt and large-amplitude climate changes in the LGM (e.g., sudden surface warming). Thiagarajan et al. (2014) provide observational evidence that intermediate water (about 1800-m depth) in the glacial North Atlantic had an abrupt warming (about 5°C) within a few hundred years, which occurred about 15 000 yr ago. This is a reversal of the ocean's usual thermal stratification, with intermediate WSW that is warmer (about 3°C; see their Fig. 1e) than the overlying CFW. Thiagarajan et al. (2014) argue that static stability of the interface requires increased salinity of the warm intermediate water. They propose that this WSW below CFW could represent potential energy for thermobaric convection (i.e., OCAPE), which might reinvigorate the Atlantic meridional overturning circulation (AMOC)

and facilitate the transition between the LGM and modern ocean stratification. We are performing an associated simulation study of these processes based on this observation and our theory of OCAPE.

Note added in proof: During the revision of this work, we found that Hieronymus and Nycander (2015) recently used the HA for some other energy diagnoses (i.e., computing the APE in their case). This implies that the HA has multiple applications for studying ocean energetics.

Acknowledgments. Z.S.'s and A.P.I.'s research was supported by NSF Award AST-1109299. A.L.S.'s research was supported by the University of California, Los Angeles. A.F.T.'s research was supported by NSF Award OCE-1235488. The author gratefully acknowledges the helpful comments from two anonymous reviewers.

REFERENCES

Adkins, J. F., A. P. Ingersoll, and C. Pasquero, 2005: Rapid climate change and conditional instability of the glacial deep ocean from the thermobaric effect and geothermal heating. *Quat. Sci. Rev.*, **24**, 581–594, doi:10.1016/j.quascirev.2004.11.005.

Akitomo, K., 1999a: Open-ocean deep convection due to thermobaricity: 1. Scaling argument. *J. Geophys. Res.*, **104**, 5225–5234, doi:10.1029/1998JC900058.

——, 1999b: Open-ocean deep convection due to thermobaricity: 2. Numerical experiments. *J. Geophys. Res.*, **104**, 5235–5249, doi:10.1029/1998JC900062.

——, 2006: Thermobaric deep convection, baroclinic instability, and their roles in vertical heat transport around Maud Rise in the Weddell Sea. *J. Geophys. Res.*, **111**, C09027, doi:10.1029/2005JC003284.

——, 2007: Restriction of convective depth in the Weddell Sea. *Geophys. Res. Lett.*, **34**, L10610, doi:10.1029/2007GL029295.

——, 2011: Two types of thermobaric deep convection possible in the Greenland Sea. *J. Geophys. Res.*, **116**, C08012, doi:10.1029/2010JC006635.

——, K. Tanaka, T. Awaji, and N. Imasato, 1995: Deep convection in a lake triggered by wind: Two-dimensional numerical experiments with a nonhydrostatic model. *J. Oceanogr.*, **51**, 171–185, doi:10.1007/BF02236523.

Arakawa, A., and W. H. Schubert, 1974: Interaction of a cumulus cloud ensemble with the large-scale environment, Part I. *J. Atmos. Sci.*, **31**, 674–701, doi:10.1175/1520-0469(1974)031<0674:IOACCE>2.0.CO;2.

Årthun, M., K. W. Nicholls, and L. Boehme, 2013: Wintertime water mass modification near an Antarctic Ice Front. *J. Phys. Oceanogr.*, **43**, 359–365, doi:10.1175/JPO-D-12-0186.1.

Bertsekas, D. P., 1988: The auction algorithm: A distributed relaxation method for the assignment problem. *Ann. Oper. Res.*, **14**, 105–123, doi:10.1007/BF02186476.

Burkard, R. E., M. Dell'Amico, and S. Martello, 2009: *Assignment Problems.* SIAM, 382 pp.

Carmack, E. C., 1979: Combined influence of inflow and lake temperatures on spring circulation in a riverine lake. *J. Phys. Oceanogr.*, **9**, 422–434, doi:10.1175/1520-0485(1979)009<0422:CIOIAL>2.0.CO;2.

——, W. J. Williams, S. L. Zimmermann, and F. A. McLaughlin, 2012: The Arctic Ocean warms from below. *Geophys. Res. Lett.*, **39**, L07604, doi:10.1029/2012GL050890.

Clarke, R. A., and J. C. Gascard, 1983: The formation of Labrador Sea water. Part I: Large-scale processes. *J. Phys. Oceanogr.*, **13**, 1764–1778, doi:10.1175/1520-0485(1983)013<1764:TFOLSW>2.0.CO;2.

Denbo, D. W., and E. D. Skyllingstad, 1996: An ocean large-eddy simulation model with application to deep convection in the Greenland Sea. *J. Geophys. Res.*, **101**, 1095–1110, doi:10.1029/95JC02828.

Derigs, U., 1985: The shortest augmenting path method for solving assignment problems? Motivation and computational experience. *Ann. Oper. Res.*, **4**, 57–102, doi:10.1007/BF02022037.

De Steur, L., D. M. Holland, R. D. Muench, and M. G. McPhee, 2007: The warm-water Halo around Maud Rise: Properties, dynamics and impact. *Deep-Sea Res. Oceanogr. Abstr.*, **54**, 871–896, doi:10.1016/j.dsr.2007.03.009.

Emanuel, K. A., J. D. Neelin, and C. S. Bretherton, 1994: On large-scale circulations in convecting atmospheres. *Quart. J. Roy. Meteor. Soc.*, **120**, 1111–1143, doi:10.1002/qj.49712051902.

Feistel, R., 2003: A new extended Gibbs thermodynamic potential of seawater. *Prog. Oceanogr.*, **58**, 43–114, doi:10.1016/S0079-6611(03)00088-0.

Garwood, R. W., Jr., S. M. Isakari, and P. C. Gallacher, 1994: Thermobaric convection. *The Polar Oceans and Their Role in Shaping the Global Environment*, *Geophys. Monogr.*, Vol. 85, Amer. Geophys. Union, 199–209.

Gordon, A. L., 1978: Deep Antarctic convection west of Maud Rise. *J. Phys. Oceanogr.*, **8**, 600–612, doi:10.1175/1520-0485(1978)008<0600:DACWOM>2.0.CO;2.

——, 1991: Two stable modes of Southern Ocean winter stratification. *Deep Convection and Deep Water Formation in the Oceans*, C. Chu and J. C. Gascard, Eds., Elsevier Oceanography Series, Vol. 57, 17–35, doi:10.1016/S0422-9894(08)70058-8.

——, and B. A. Huber, 1990: Southern Ocean winter mixed layer. *J. Geophys. Res.*, **95**, 11 655–11 672, doi:10.1029/JC095iC07p11655.

——, and ——, 1995: Warm Weddell deep water west of Maud Rise. *J. Geophys. Res.*, **100**, 13 747–13 753, doi:10.1029/95JC01361.

——, A. H. Orsi, R. Muench, B. A. Huber, E. Zambianchi, and M. Visbeck, 2009: Western Ross Sea continental slope gravity currents. *Deep-Sea Res. II*, **56**, 796–817, doi:10.1016/j.dsr2.2008.10.037.

Gregory, D., J. J. Morcrette, C. Jakob, A. C. M. Beljaars, and T. Stockdale, 2000: Revision of convection, radiation and cloud schemes in the ECMWF integrated forecasting system. *Quart. J. Roy. Meteor. Soc.*, **126**, 1685–1710, doi:10.1002/qj.49712656607.

Harcourt, R. R., 2005: Thermobaric cabbeling over Maud Rise: Theory and large eddy simulation. *Prog. Oceanogr.*, **67**, 186–244, doi:10.1016/j.pocean.2004.12.001.

——, E. L. Steffen, R. W. Garwood, and E. A. D'Asaro, 2002: Fully Lagrangian floats in Labrador Sea deep convection: Comparison of numerical and experimental results. *J. Phys. Oceanogr.*, **32**, 493–510, doi:10.1175/1520-0485(2002)032<0493:FLFILS>2.0.CO;2.

Hieronymus, M., and J. Nycander, 2015: Finding the minimum potential energy state by adiabatic parcel rearrangements with a nonlinear equation of state: An exact solution in polynomial time. *J. Phys. Oceanogr.*, **45**, 1843–1857, doi:10.1175/JPO-D-14-0174.1.

Hoppema, M., E. Fahrbach, G. Rohardt, and A. Wisotzki, 2006: Warm events and ice cover near Maud Rise, Weddell Sea. *Geophysical Research Abstracts*, Vol. 8, Abstract 04398.

[Available online at http://meetings.copernicus.org/www.cosis.net/abstracts/EGU06/04398/EGU06-J-04398.pdf.]

Huang, R. X., 2005: Available potential energy in the world's oceans. *J. Mar. Res.*, **63**, 141–158, doi:10.1357/0022240053693770.

Ingersoll, A. P., 2005: Boussinesq and anelastic approximations revisited: Potential energy release during thermobaric instability. *J. Phys. Oceanogr.*, **35**, 1359–1369, doi:10.1175/JPO2756.1.

IOC, SCOR, and IAPSO, 2010: The International Thermodynamic Equation of Seawater—2010: Calculation and use of thermodynamic properties. Intergovernmental Oceanographic Commission, Manuals and Guides 56, 220 pp. [Available online at http://www.teos-10.org/pubs/TEOS-10_Manual.pdf.]

Jackett, D. R., T. J. McDougall, R. Feistel, D. G. Wright, and S. M. Griffies, 2006: Algorithms for density, potential temperature, conservative temperature, and the freezing temperature of seawater. *J. Atmos. Oceanic Technol.*, **23**, 1709–1728, doi:10.1175/JTECH1946.1.

Krokhmal, P. A., and P. M. Pardalos, 2009: Random assignment problems. *Eur. J. Oper. Res.*, **194**, 1–17, doi:10.1016/j.ejor.2007.11.062.

Kuhn, H. W., 1955: The Hungarian method for the assignment problem. *Nav. Res. Logist.*, **2**, 83–97, doi:10.1002/nav.3800020109.

Labeyrie, L. D., J. C. Duplessy, J. Duprat, A. Juillet-Leclerc, J. Moyes, E. Michel, N. Kallel, and N. J. Shackleton, 1992: Changes in the vertical structure of the North Atlantic Ocean between glacial and modern times. *Quat. Sci. Rev.*, **11**, 401–413, doi:10.1016/0277-3791(92)90022-Z.

Lange, M. A., S. F. Ackley, P. Wadhams, G. S. Dieckmann, and H. Eicken, 1989: Development of sea ice in the Weddell Sea. *Ann. Glaciol.*, **12**, 92–96.

Lawler, E. L., 1976: *Combinatorial Optimization: Networks and Matroids.* Holt, Rinehart and Winston, 374 pp.

Macdonald, A. M., and C. Wunsch, 1996: An estimate of global ocean circulation and heat fluxes. *Nature*, **382**, 436–439, doi:10.1038/382436a0.

Marshall, J., and F. Schott, 1999: Open-ocean convection: Observations, theory, and models. *Rev. Geophys.*, **37**, 1–64, doi:10.1029/98RG02739.

Martello, S., and P. Toth, 1987: Linear assignment problems. *Surveys in Combinatorial Optimization*, S. Martello et al., Eds., North-Holland Mathematics Studies, Vol. 132, Elsevier, 259–282.

——, D. Pisinger, and D. Vigo, 2000: The three-dimensional bin packing problem. *Oper. Res.*, **48**, 256–267, doi:10.1287/opre.48.2.256.12386.

McDougall, T. J., 1987: Thermobaricity, cabbeling, and water-mass conversion. *J. Geophys. Res.*, **92**, 5448–5464, doi:10.1029/JC092iC05p05448.

McPhee, M. G., 2000: Marginal thermobaric stability in the ice-covered upper ocean over Maud Rise. *J. Phys. Oceanogr.*, **30**, 2710–2722, doi:10.1175/1520-0485(2000)030<2710:MTSITI>2.0.CO;2.

——, 2003: Is thermobaricity a major factor in Southern Ocean ventilation? *Antarct. Sci.*, **15**, 153–160, doi:10.1017/S0954102003001159.

——, and Coauthors, 1996: The Antarctic zone flux experiment. *Bull. Amer. Meteor. Soc.*, **77**, 1221–1232, doi:10.1175/1520-0477(1996)077<1221:TAZFE>2.0.CO;2.

Parkinson, C. L., and D. J. Cavalieri, 2012: Antarctic sea ice variability and trends, 1979–2010. *Cryosphere*, **6**, 871–880, doi:10.5194/tc-6-871-2012.

Reddy, J. N., 2002: *Energy Principles and Variational Methods in Applied Mechanics.* 2nd ed. John Wiley and Sons, 592 pp.

Reid, R. O., B. A. Elliott, and D. B. Olson, 1981: Available potential energy: A clarification. *J. Phys. Oceanogr.*, **11**, 15–29, doi:10.1175/1520-0485(1981)011<0015:APEAC>2.0.CO;2.

Renfrew, I., J. C. King, and T. Markus, 2002: Coastal polynyas in the southern Weddell Sea: Variability of the surface energy budget. *J. Geophys. Res.*, **107**, doi:10.1029/2000JC000720.

Salby, M. L., 1996: Fundamentals of Atmospheric Physics. International Geophysics Series, Vol. 61, Academic Press, 627 pp.

Schmid, M., N. M. Budnev, N. G. Granin, M. Sturm, M. Schurter, and A. Wüest, 2008: Lake Baikal deepwater renewal mystery solved. *Geophys. Res. Lett.*, **35**, L09605, doi:10.1029/2008GL033223.

Schott, F., and K. D. Leaman, 1991: Observations with moored acoustic Doppler current profilers in the convection regime in the Golfe du Lion. *J. Phys. Oceanogr.*, **21**, 558–574, doi:10.1175/1520-0485(1991)021<0558:OWMADC>2.0.CO;2.

——, M. Visbeck, and J. Fischer, 1993: Observations of vertical currents and convection in the central Greenland Sea during the winter of 1988–1989. *J. Geophys. Res.*, **98**, 14 401–14 421, doi:10.1029/93JC00658.

Su, Z., A. L. Stewart, and A. F. Thompson, 2014: An idealized model of Weddell Gyre export variability. *J. Phys. Oceanogr.*, **44**, 1671–1688, doi:10.1175/JPO-D-13-0263.1.

——, A. P. Ingersoll, A. L. Stewart, and A. F. Thompson, 2016: Ocean convective available potential energy. Part II: Energetics of thermobaric convection and thermobaric cabbeling. *J. Phys. Oceanogr.*, **46**, 1097–1115, doi:10.1175/JPO-D-14-0156.1.

Talley, L. D., V. Lobanov, V. Ponomarev, A. Salyuk, P. Tishchenko, I. Zhabin, and S. Riser, 2003: Deep convection and brine rejection in the Japan Sea. *Geophys. Res. Lett.*, **30**, 1159, doi:10.1029/2002GL016451.

——, P. Tishchenko, V. Luchin, A. Nedashkovskiy, S. Sagalaev, D. J. Kang, M. Warner, and D. H. Min, 2004: Atlas of Japan (East) Sea hydrographic properties in summer, 1999. *Prog. Oceanogr.*, **61**, 277–348, doi:10.1016/j.pocean.2004.06.011.

Thiagarajan, N., A. V. Subhas, J. R. Southon, J. M. Eiler, and J. F. Adkins, 2014: Abrupt pre-Bølling–Allerød warming and circulation changes in the deep ocean. *Nature*, **511**, 75–78, doi:10.1038/nature13472.

Trenberth, K., 2005: Uncertainty in hurricanes and global warming. *Science*, **308**, 1753–1754, doi:10.1126/science.1112551.

Vallis, G. K., 2006: *Atmospheric and Oceanic Fluid Dynamics: Fundamentals and Large-Scale Circulation.* Cambridge University Press, 745 pp.

Wadhams, P., J. Holfort, E. Hansen, and J. P. Wilkinson, 2002: A deep convective chimney in the winter Greenland Sea. *Geophys. Res. Lett.*, **29**, doi:10.1029/2001GL014306.

Weiss, R. F., E. C. Carmack, and V. M. Koropalov, 1991: Deep-water renewal and biological production in Lake Baikal. *Nature*, **349**, 665–669, doi:10.1038/349665a0.

Winters, K. B., P. N. Lombard, J. J. Riley, and E. A. D'Asaro, 1995: Available potential energy and mixing in density-stratified fluids. *J. Fluid Mech.*, **289**, 115–128, doi:10.1017/S002211209500125X.

Young, W. R., 2010: Dynamic enthalpy, conservative temperature, and the seawater Boussinesq approximation. *J. Phys. Oceanogr.*, **40**, 394–400, doi:10.1175/2009JPO4294.1.

Zhang, G. J., 2009: Effects of entrainment on convective available potential energy and closure assumptions in convection parameterization. *J. Geophys. Res.*, **114**, D07109, doi:10.1029/2008JD010976.

——, and N. A. McFarlane, 1995: Sensitivity of climate simulations to the parameterization of cumulus convection in the Canadian Climate Centre general circulation model. *Atmos.–Ocean*, **33**, 407–446, doi:10.1080/07055900.1995.9649539.